

# Model-independent determination of the Migdal effect via photoabsorption

C.-P. Liu,<sup>1,\*</sup> Chih-Pan Wu,<sup>2,†</sup> Hsin-Chang Chi,<sup>1,‡</sup> and Jiunn-Wei Chen<sup>3,§</sup>

<sup>1</sup>*Department of Physics, National Dong Hwa University, Shoufeng, Hualien 974301, Taiwan*

<sup>2</sup>*Département de physique, Université de Montréal, Montréal, H3C 3J7, Canada*

<sup>3</sup>*Department of Physics, Center for Theoretical Physics,  
and Leung Center for Cosmology and Particle Astrophysics,  
National Taiwan University, Taipei 10617, Taiwan*

(Dated: July 22, 2020)

The Migdal effect in a dark-matter-nucleus scattering extends the direct search experiments to the sub-GeV mass region through electron ionization with sub-keV detection thresholds. In this paper, we derive a rigorous and model-independent “Migdal-photoabsorption” relation that links the sub-keV Migdal process to photoabsorption. This relation is free of theoretical uncertainties as it only requires the photoabsorption cross section as the experimental input. Validity of this relation is explicitly checked in the case of xenon with a state-of-the-arts atomic calculation that is well-benchmarked by experiments. The predictions based on this relation for xenon, argon, semiconductor silicon and germanium detectors are presented and discussed.

*Introduction.* Direct searches for the weakly-interacting massive particle (WIMP), one of the favorite dark matter (DM) candidates, has been making tremendous progress in recent years: In the mass range of  $m_\chi \sim 10 - 100$  GeV,<sup>1</sup> the limits on its spin-independent scattering cross section off nucleon reach down to the range of  $\sigma_n \lesssim 10^{-46} - 10^{-47}$  cm<sup>2</sup>; in the mass range of 1 – 10 GeV, the limits are also improving, however, not as stringent as in the heavier case (see, e.g., Ref. [1] for a recent review). The obvious reason is a lighter WIMP has less kinetic energy so it is less probable to generate observable nuclear recoil (NR) events from WIMP-nucleus scattering. Ultimately, a detector’s NR threshold cuts off any sensitivity to  $m_\chi$  below a certain value, as seen in every WIMP exclusion plot.

To expand a direct detector’s coverage of low-mass WIMPs, or more generically light dark matter (LDM), a recent proposal by Ibe et al. [2] that uses the so-called Migdal effect has attracted great interests. This effect, first noted by A. B. Migdal [3], refers to an inelastic exit channel in scattering off an atomic nucleus, where not only the atomic center of mass gets recoil (typically termed as NR) but also the intrinsic atomic electron state is excited or ionized. Unlike the elastic exit channel, the Migdal effect generates other electromagnetic signals in the form of ionized electrons and photons from atomic de-excitation or recombination, which are more energetic than NR hence is detectable. This novel DM detection mode has been applied to several experiments [4–10] and some of them give the current best limits on DM-nucleus interactions in the mass range below GeV. With detectors of larger size and longer data taking time, e.g., xenon-based XENONnT [11], LZ [12], and DARWIN [13]; argon-based DarkSide [14], DEAP [15], and ArDM [16]; or of lower threshold and better resolution,

e.g., germanium-based EDELWEISS [17] and CDMS HVeV [18]; silicon-based SENSEI [19] and DAMIC [20], the Migdal effect will be a promising probe of hadrophilic LDM.

While detecting the Migdal effect is an experimental challenge, predicting its count rate is mostly a theoretical one [2, 21–23]. For a relic sub-GeV LDM candidate, its kinetic energy is no bigger than  $\sim$  keV, so the scattering process falls in the atomic scale. Proper understanding of such a sub-keV Migdal effect inevitably involves atomic physics. The lower the energy, the more pronounced many-body effects are expected. The complexity of many-body physics adds a new layer when detector media can no longer be treated as isolated atoms. This means at certain low-energy levels it will be necessary to take into account molecular or condensed-matter physics, depending on a detector’s material phase. All these problems are highly non-trivial but essential.

To address the theory issues related to the Migdal effect, we first derive a relation that links the low-energy Migdal process to photoabsorption, which is exact at the long wavelength limit of photon and expected to work up to  $\sim$  keV. The relation has two major advantages: it applies to all kinds of DM detectors in general, and is free of theoretical uncertainties because only photoabsorption cross section (experimentally measurable!) is needed for input. To demonstrate the robustness of this relation, we study the case of xenon by applying a state-of-the-art atomic approach, the relativistic random phase approximation (RRPA), whose high precision has been demonstrated in Ref. [24]. Finally we use this relation to predict the Migdal effects in argon, silicon, and germanium detectors.

*Migdal effect.* The transition operator and matrix element of a Migdal process has been derived in several ways, e.g., through a sudden approximation [25], non-relativistic scattering with Galilean invariance [26] (for hydrogen-like systems), and relativistic scattering with

<sup>1</sup> We use the natural units  $\hbar = c = 1$  exclusively in this paper.

full Lorentz covariance [2]. Because of the hierarchy between atomic, nuclear, electron mass,  $m_A$ ,  $m_N$ ,  $m_e$ , and atomic binding energy  $E_B$ :  $m_A \approx m_N \gg m_e \gg E_B$ , all derivations converge on the resulting Migdal matrix element

$$M_{FI} = \left\langle F \left| e^{-i\frac{m_e}{m_A}\vec{q}_A \cdot \sum_{i=1}^Z \vec{r}_i} \right| I \right\rangle, \quad (1)$$

where  $\vec{q}_A$  is the 3-momentum transfer to the atomic system;  $\vec{r}_i$  the coordinate of the  $i$ th electron;  $|I\rangle$  and  $|F\rangle$  the atomic initial and final states in the intrinsic frame (i.e., with the center of mass motion being factored out), respectively.<sup>2</sup>

First, notice that the summation over all  $Z$  electron coordinates appears in the exponent, so the  $n$ th-order series expansion contains  $n$ -body operators, whose matrix elements are tedious to compute. By a naïve dimensional analysis:  $|\vec{q}_A| \sim m_\chi v_\chi$  with DM velocity  $v_\chi \sim 10^{-3}$ ; and  $\langle \vec{r}_i \rangle \sim (Z_i m_e \alpha)^{-1}$  with  $Z_i$  being the effective charge seen by the  $i$ th electron and  $\alpha$  the fine structure constant, one can define an atomic-shell-dependent expansion parameter  $\epsilon_i = \frac{m_\chi v_\chi}{m_A} \frac{1}{\alpha Z_i}$ . In the case of xenon,  $m_A \sim 120 \text{ GeV}$ , so  $\epsilon_i \sim \frac{0.001 m_\chi}{Z_i \text{ GeV}}$  guarantees good convergence for sub-GeV DM even with a  $Z_i = 1$  assumption. In reality, current xenon detector thresholds are  $\sim \text{keV}$ , most Migdal events would be from inner-shell ionizations with  $Z_i$  surely larger than 1. Therefore, for LDM searches, the Migdal matrix element can be well-approximated by the leading-order term

$$M_{FI}^{(1)} = -i \frac{m_e}{m_A} \vec{q}_A \cdot \left\langle F \left| \sum_{i=1}^Z \vec{r}_i \right| I \right\rangle \equiv -i \frac{m_e}{m_A} \vec{q}_A \cdot \vec{D}_{FI}, \quad (2)$$

where  $\vec{D}_{FI}$  is the familiar dipole matrix element.

The energy deposition by DM in a Migdal process goes into two parts: one to the atomic center-of-mass kinetic energy (or the NR energy),  $E_R$ , and the other to the atomic discrete excitation or ionization, denoted as  $E_r = E_F - E_I$  while  $E_{F(I)}$  the eigenenergy of the state  $|F(I)\rangle$ . To accommodate different DM detector's approaches in measuring the combinations of  $E_R$  and  $E_r$ , it is customary to cast the cross section in a double differential form

$$\frac{d\sigma}{dE_R dE_r} = \frac{m_e^2}{\mu_N^2 v_\chi^2} \tilde{\sigma}_N(q_A) E_R \overline{D_{FI}^2}, \quad (3)$$

where  $\mu_N = m_N m_\chi / (m_N + m_\chi)$  is the reduced mass of the DM-nucleus system, and  $\tilde{\sigma}_N$  the DM-nucleus cross section which depends on  $q_A = \sqrt{2m_A E_R}$ . The averaged dipole matrix element squared  $\overline{D_{FI}^2}$  involves a summation

of all allowed final states and an average of degenerate initial states.<sup>3</sup>

*Photoabsorption and its relation to the Migdal effect.* As seen from Eq. 3, the quantity  $\overline{D_{FI}^2}$  is the critical piece of information that requires many-body calculations. Therefore, it is desirable to ask whether it can be extracted directly from experiments. Fortunately, photoabsorption provides the answer.

The full transition matrix element for photoabsorption takes the form

$$P_{FI} = \hat{\epsilon} \cdot \left\langle F \left| \sum_{i=1}^Z e^{i\vec{k} \cdot \vec{r}_i} \vec{\alpha}_i \right| I \right\rangle \equiv \hat{\epsilon} \cdot \vec{O}_{FI}, \quad (4)$$

where  $\vec{k}$  and  $\hat{\epsilon}$  are the photon momentum and polarization vectors, and  $\vec{\alpha}_i$  the  $4 \times 4$  spatial Dirac matrix. By energy conservation, the photon energy  $\omega = |\vec{k}| = E_r$  (the atomic recoil is negligible as  $\omega \ll m_A$ ). The total cross section of photoabsorption is

$$\sigma_\gamma(E_r) = \frac{4\pi^2 \alpha}{E_r} \overline{P_{FI}^2}, \quad (5)$$

where the same summation and average of states being applied to  $P_{FI}$  as in the case to  $D_{FI}$ .

The standard procedure of calculating  $\sigma_\gamma(E_r)$  starts by a multipole expansion of  $P_{FI}$  that yields the transverse electric,  $T_J^{el}(kr)$ , and transverse magnetic,  $T_J^{mag}(kr)$ , multipoles with  $J = 1, 2, \dots$  denoting the spherical multipolarity. At the long wavelength (LW) limit, i.e.,  $k \langle r \rangle \ll 1$  so that  $e^{i\vec{k} \cdot \vec{r}} \rightarrow 1$ , the transition matrix element is simplified to

$$\vec{O}_{FI}^{(E1)} = \left\langle F \left| \sum_{i=1}^Z \vec{\alpha}_i \right| I \right\rangle \equiv \vec{D}_{FI}^{(V)} = i E_r \vec{D}_{FI}. \quad (6)$$

This is the electric dipole (E1) approximation for photoabsorption, as the resulting atomic operator is a parity-odd dipole, either as  $\vec{\alpha}_i$ , usually termed as the velocity form (denoted by the superscript ‘‘V’’), or  $\vec{r}_i$ , the length form. The equivalence of these two operators is established by the commutation relation  $-i[\vec{r}_i, H] = \vec{\alpha}_i$ . As a result,  $\sigma_\gamma(E_r)$  can be approximated by

$$\sigma_\gamma(E_r) \xrightarrow{E1 \text{ approx.}} 4\pi^2 \alpha E_r \overline{D_{FI}^2}, \quad (7)$$

and the Migdal differential cross section can be cast into

$$\frac{d\sigma^{(\text{MPA})}}{dE_R dE_r} = \frac{m_e^2}{\mu_N^2 v_\chi^2} \tilde{\sigma}_N(q_A) \frac{E_R}{E_r} \frac{\sigma_\gamma(E_r)}{4\pi^2 \alpha}, \quad (8)$$

<sup>2</sup> In this work, atomic states are treated relativistically, so the Migdal operator is a  $4 \times 4$  diagonal matrix.

<sup>3</sup> Our choice of wave function normalization is  $\langle E_I | E_I \rangle = \delta_{II'}$  for bound states and  $\langle E_F | E_{F'} \rangle = \delta(E_F - E_{F'})$  for continuum states.

which we call the ‘‘Migdal-photoabsorption’’ (MPA) relation. This relation is powerful: it tells that as long as the photoabsorption cross section can be measured in a detector, the corresponding Migdal effect can be figured accordingly, and there is no need for theory input. In contrast, the relation proposed in Ref. [22] involves DM-electron scattering, which is yet to be detected.

While the derivation of the  $E1$  approximation is straightforward, there are two points of particular importance from a theory viewpoint. First, at the LW limit, all the so-called retardation effects from  $e^{i\vec{k}\cdot\vec{r}} - 1$  are ignored. They are grouped into higher-rank spherical multipoles or higher-order corrections (in powers of  $k^2 r^2$ ) to spherical multipoles of a given rank.

Second, the equivalence between the dipole operators in the velocity and length forms, manifested here by a simple commutation relation, has a deeper connection to the gauge invariance of electromagnetism. As first noted by Siegert [27], the transverse electric multipole operators can be related by current conservation to the charge multipole operators at the LW limit. However, the equivalence at the matrix-element level has an additional requirement that the wave functions are energy eigenstates, i.e.,  $H|F(I)\rangle = E_{F(I)}|F(I)\rangle$ . For most many-body calculations that only approximate the true eigenstates, the breaking of gauge invariance, e.g.,  $\bar{D}_{FI}^{(V)} \neq \bar{D}_{FI}$ , is quite commonly seen. Therefore, adopting many-body approaches that preserve gauge invariance, such as (R)RPA [28],<sup>4</sup> is preferred. Conversely, the degree of broken gauge invariance can serve as a robustness test of a many-body calculation. In atomic physics, this is usually done with two different forms of  $T_J^{el}$ , one in the Coulomb gauge and the other the ‘‘length gauge’’ [29].

*Case study of xenon.* In Fig. 1, the experimental data for xenon photoabsorption, compiled from Refs. [30–34], are compared with several theoretical calculations. The agreement between the RRPA curve, taken from Ref. [24] using operators in the length gauge, shows that our atomic approach can handle many-body excited states properly. In this work, we carry out two additional calculations: one with the  $E1$  approximation, i.e., Eq. (7), and the other with operators in the Coulomb gauge. As shown in the central panel, the  $E1$  approximation works very well up to 1 keV with all higher-order corrections still kept at a level below 1%. This justifies the basic assumption underlying the MPA relation: the averaged dipole matrix element squared  $\bar{D}_{FI}^2$  in the sub-keV Migdal process can be reliably extracted from photoabsorption measurements. In the bottom panel, the nontrivial property of gauge invariance in many-body calculations is clearly shown to be preserved by the RRPA approach.

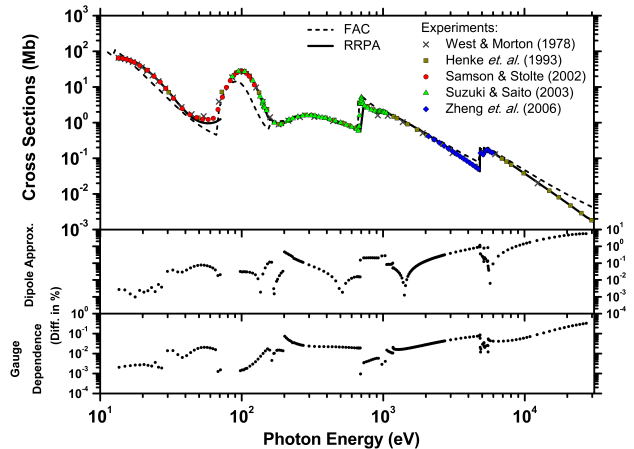


FIG. 1. (Top panel) Xenon photoabsorption cross section from experiments and atomic calculations of RRPA with the length-gauge operators and the FAC code. Also shown are the percentage differences by using the  $E1$  approximation (central panel) and from using the Coulomb gauge operators (bottom panel) in the same RRPA routine.

The FAC results are obtained by running a built-in module in the ‘‘Flexible Atomic Code’’ package that calculates photoionization cross sections directly [35]. As the comparison shows, the FAC code does a reasonably good job for  $E_r \gtrsim 200$  eV in general, but at lower energies, it does not perform well, and errors at some points are quite large. By construct, the FAC package is mainly designed for highly-ionized atoms and built with focus on efficiency instead of accuracy. Therefore, its many-body approach is solving a prescribed form of averaged one-body potential (in this sense, not an *ab initio* approach) self-consistently, and leads to a picture that all electrons act like independent particles, which is unrealistic at low energies. Another noteworthy point is for  $E_r \gtrsim 1$  keV, FAC has the tendency to over-predict when  $E_r$  gets away from edge energies. This is because the transition operators being adopted, except  $T_1^{mag}$ , are non-relativistic, and contributions from all sub-leading orders in  $k^2 r^2$  are missing.

For prediction of Migdal count rates, we follow the same procedures as in Ref. [2] and [22]. In the former case, the observable energy  $E_{det}$  is a sum of  $E_r$  and  $q_{nr} E_R$  with  $q_{nr}$  the NR quenching factor, and the differential count rate is

$$\frac{dR}{dE_{det}} = n_\chi N_T \int dE_R \int dE_r \delta(E_{det} - q_{nr} E_R - E_r) \times \tilde{\sigma}_N(q_A) E_R \bar{D}_{FI}^2 \eta(v_{min}). \quad (9)$$

For the latter case, the observable energy is  $E_r$  and the

<sup>4</sup> In the same paper [28], the most commonly-used Hartree-Fock method is shown to violate gauge invariance.

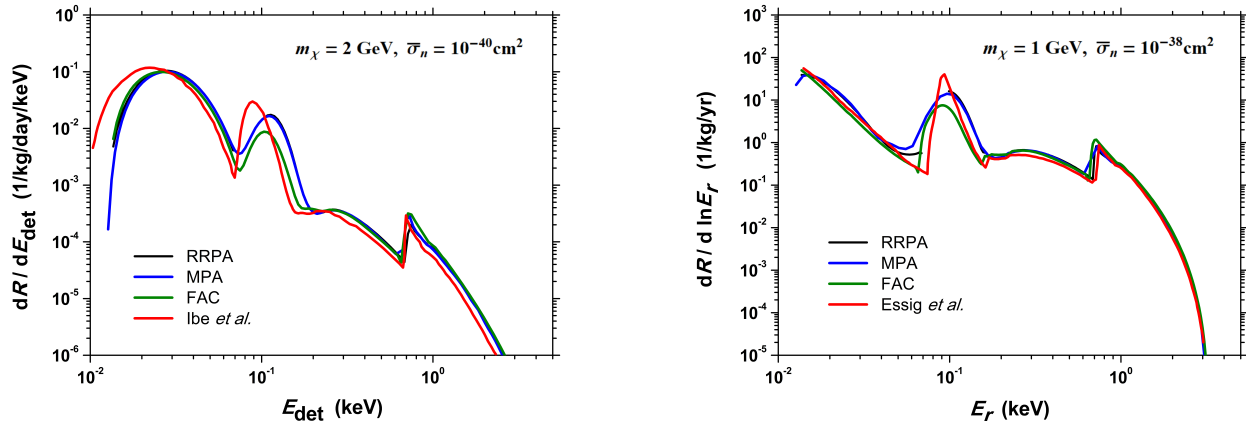


FIG. 2. Differential count rates  $\frac{dR}{dE_{\text{det}}}$  (left) and  $\frac{dR}{d \ln E_r}$  (right) of the Migdal effect in xenon detectors by the spin-independent, isoscalar, DM-nucleon contact interaction (with cross section  $\bar{\sigma}_n$ ) predicted by (i) RRPA, (ii) MPA relation, (iii) FAC, and (iv) Ref. [2] (left) and Ref. [22] (right).

differential count rate is simply

$$\frac{dR}{dE_r} = n_\chi N_T \frac{m_e^2}{\mu_N^2} \overline{D^2}_{FI} \int dE_R \tilde{\sigma}_N(q_A) E_R \eta(v_{\min}), \quad (10)$$

where  $n_\chi$  is the local DM number density,  $N_T$  the number of target atoms, and the  $\eta$  function results from the  $1/v_\chi$  factor averaged with the DM velocity spectrum [36], and depends on the minimum DM velocity  $v_{\min} = (m_N E_R + \mu_N E_r) / (\mu_N \sqrt{2m_N E_R})$  that guarantees energy deposition of  $E_R + E_r$  is possible.

In Fig. 2, we plot four sets of count rate predictions assuming a contact, spin-independent, isoscalar DM-nucleus interaction so that  $\tilde{\sigma}_N = A^2 \mu_N^2 \mu_n^{-2} \bar{\sigma}_n$  with  $\mu_n$  being the DM-nucleon reduced mass and  $\bar{\sigma}_n$  the DM-nucleon cross section: The black line is by direct computation of Eq. (3) using RRPA; the blue (green) line is obtained by the MPA relation with  $\sigma_\gamma(E_r)$  taken from data (FAC). The nice agreement between RRPA and MPA is not only a justification to the applicability of the MPA relation, but also a theory-experiment double confirmation of the results. The difference between our results from the ones of Refs. [2, 22] are most likely originated from different atomic approaches. Generally speaking, mean field methods can give good results of ground state properties and wave functions, but their applicability to excited states can be problematic. Note that Ref. [2] used the FAC package differently from what we do. The authors adopted the picture that the atomic excited states are purely 1-particle-1-hole excitations (because the leading-order Migdal operator is one-body) from the ground state. This independent particle picture ignores not only the residual two-body correlation, but also the fact that atomic mean field varies with electronic configuration. The FAC package takes into account the

latter aspect by diagonalizing the atomic Hamiltonian in the model space of a given problem. The resulting wave functions are configuration-mixed, i.e., not in form of a single Slater determinant. This explains why the FAC results are closer to our RRPA results than Ref. [2].

*Applications to argon, silicon, and germanium detectors.* Using the MPA relation, we combine in Fig. 3 the predicted count rates for xenon, argon, semiconductor silicon and germanium detectors. For  $E_r \geq 10$  eV, the measured photoabsorption data are taken from Ref. [31] along with semi-empirical fitting; for semiconductor silicon and germanium at room temperature and  $1 \text{ eV} < E_r < 10 \text{ eV}$ , they are from Ref. [37] and [38], respectively. The silicon prediction roughly agrees with the one of Ref. [22], which is based on a detailed condensed matter calculation. The difference in the 1 – 5 eV region could be from the many-body computation or because the photoabsorption data being used do not exactly apply to the case of the SENSEI detector. The argon prediction should be robust, unlike the large theoretical uncertainties assigned in Ref. [39] based on the atomic calculation of Ref. [2].

More impressively, the MPA relation provides a reliable germanium prediction in the energy range of 1 – 80 eV. According to our previous study of atomic germanium [40, 41], the MCRRPA method (the RRPA with multiconfiguration required for open-shell atoms), though sophisticated enough, does not work satisfactorily in this energy because the crystal effects. Now, it is no longer an obstacle, and the experimental analyses, such as being done by EDELWEISS [7] and CDEX [8], can include these shells, which have dominant contributions for  $E_r < 100$  eV. Another significant feature is that the germanium detector can be very sensitive to the Migdal effect at extremely low energy, because of its spe-

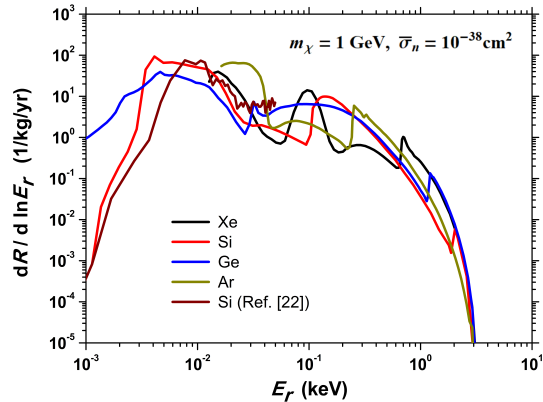


FIG. 3. Differential count rates  $\frac{dR}{d \ln E_r}$  for xenon, argon, semiconductor silicon and germanium detectors.

cially large photoabsorption coefficient in  $E_r = 1 - 3$  eV. Both CDMS HVeV [18] and EDELWEISS [17] recently demonstrate their extremely-low-threshold capability at 1 eV. According to the plot, the Migdal count rate can be 3-order-of-magnitude bigger than in a silicon detector, assuming equal exposure mass-time.

It should also be pointed out that different detectors complement one another, thanks to the rich atomic structure. At each photoabsorption peak, the cross section and the resulting Migdal rate can receive a substantial boost. This not only enhances the sensitivity but also provides smoking gun signatures.

*Conclusion.* The Migdal effect has been a powerful search mode for hadrophilic, sub-GeV light dark matter. With modern technologies pushing detector thresholds lower and lower, our range of light dark matter searches will expand further. The “Migdal-photoabsorption” relation we derived in this work is based on general principles and only requires photoabsorption measurements as input. It thus provides predictions that have no uncertainties from many-body calculations. Though we only consider xenon, argon, semiconductor silicon and germanium detectors as examples, it certainly can be applied to other novel low-threshold detectors.

This work is supported in part under Grant Nos. 108-2112-M-259-003 (CPL) , 108-2112-M-002-003-MY3 (JWC) from the Ministry of Science and Technology, 2019-20/ECP-2 from the National Center of Theoretical Sciences, and Kenda Foundation (JWC) of Taiwan; and the Canada First Research Excellence Fund through the Arthur B. McDonald Canadian Astroparticle Physics Research Institute (CPW).

\* cpliu@mail.ndhu.edu.tw

† chih-pan.wu@umontreal.ca  
‡ hsinchang@gms.ndhu.edu.tw  
§ jwc@phys.ntu.edu.tw

- [1] P. A. Zyla *et al.* (Particle Data Group), Prog. Theor. Exp. Phys. , 083C01 (2020), to be published.
- [2] M. Ibe, W. Nakano, Y. Shoji, and K. Suzuki, *JHEP* **03**, 194 (2018), arXiv:1707.07258 [hep-ph].
- [3] A. B. Migdal, *ZhETF* **9**, 1163 (1939).
- [4] M. J. Dolan, F. Kahlhoefer, and C. McCabe, *Phys. Rev. Lett.* **121**, 101801 (2018), arXiv:1711.09906 [hep-ph].
- [5] M. Kobayashi *et al.* (XMASS), *Phys. Lett. B* **795**, 308 (2019), arXiv:1808.06177 [astro-ph.CO].
- [6] D. Akerib *et al.* (LUX), *Phys. Rev. Lett.* **122**, 131301 (2019), arXiv:1811.11241 [astro-ph.CO].
- [7] E. Armengaud *et al.* (EDELWEISS), *Phys. Rev. D* **99**, 082003 (2019), arXiv:1901.03588 [astro-ph.GA].
- [8] Z. Liu *et al.* (CDEX), *Phys. Rev. Lett.* **123**, 161301 (2019), arXiv:1905.00354 [hep-ex].
- [9] E. Aprile *et al.* (XENON), *Phys. Rev. Lett.* **123**, 241803 (2019), arXiv:1907.12771 [hep-ex].
- [10] L. Barak *et al.* (SENSEI), (2020), arXiv:2004.11378 [astro-ph.CO].
- [11] E. Aprile *et al.* (XENON), (2020), arXiv:2007.08796 [physics.ins-det].
- [12] D. Akerib *et al.* (LZ), *Nucl. Instrum. Meth. A* **953**, 163047 (2020), arXiv:1910.09124 [physics.ins-det].
- [13] J. Aalbers *et al.* (DARWIN), *JCAP* **11**, 017 (2016), arXiv:1606.07001 [astro-ph.IM].
- [14] C. Aalseth *et al.*, *Adv. High Energy Phys.* **2015**, 541362 (2015).
- [15] P.-A. Amaudruz *et al.* (DEAP-3600), *Astropart. Phys.* **108**, 1 (2019), arXiv:1712.01982 [astro-ph.IM].
- [16] J. Calvo *et al.* (ArDM), *JCAP* **03**, 003 (2017), arXiv:1612.06375 [physics.ins-det].
- [17] Q. Arnaud *et al.* (EDELWEISS), (2020), arXiv:2003.01046 [astro-ph.GA].
- [18] R. Agnese *et al.* (SuperCDMS), *Phys. Rev. Lett.* **121**, 051301 (2018), [Erratum: *Phys.Rev.Lett.* **122**, 069901 (2019)], arXiv:1804.10697 [hep-ex].
- [19] O. Abramoff *et al.* (SENSEI), *Phys. Rev. Lett.* **122**, 161801 (2019), arXiv:1901.10478 [hep-ex].
- [20] A. Aguilar-Arevalo *et al.* (DAMIC), *Phys. Rev. Lett.* **123**, 181802 (2019), arXiv:1907.12628 [astro-ph.CO].
- [21] N. F. Bell, J. B. Dent, J. L. Newstead, S. Sabharwal, and T. J. Weiler, *Phys. Rev. D* **101**, 015012 (2020), arXiv:1905.00046 [hep-ph].
- [22] R. Essig, J. Pradler, M. Sholapurkar, and T.-T. Yu, *Phys. Rev. Lett.* **124**, 021801 (2020), arXiv:1908.10881 [hep-ph].
- [23] D. Baxter, Y. Kahn, and G. Krnjaic, *Phys. Rev. D* **101**, 076014 (2020), arXiv:1908.00012 [hep-ph].
- [24] J.-W. Chen, H.-C. Chi, C.-P. Liu, and C.-P. Wu, *Phys. Lett. B* **774**, 656 (2017), arXiv:1610.04177 [hep-ex].
- [25] L. D. Landau and E. M. Lifshitz, *Quantum Mechanics (Non-relativistic Theory)* (Butterworth Heinemann, Oxford, 1991).
- [26] J.-W. Chen, H.-C. Chi, C. P. Liu, C.-L. Wu, and C.-P. Wu, *Phys. Rev. D* **92**, 096013 (2015), arXiv:1508.03508 [hep-ph].
- [27] A. Siegert, *Phys. Rev.* **56**, 750 (1939).
- [28] D. L. Lin, *Phys. Rev. A* **16**, 600 (1977).
- [29] I. P. Grant, *J. Phys. B* **7**, 1458 (1974).
- [30] J. B. West and J. Morton, *At. Data Nucl. Data Tables* **22**, 103 (1978).

- [31] B. L. Henke, E. M. Gullikson, and J. C. Davis, *Atom. Data Nucl. Data Tabl.* **54**, 181 (1993).
- [32] J. Samson and W. Stolte, *J. Electron Spectrosc. Relat. Phenom.* **123**, 265 (2002).
- [33] I. H. Suzuki and N. Saito, *J. Electron Spectrosc. Relat. Phenom.* **129**, 71 (2003).
- [34] L. Zheng, M. Cui, Y. Zhao, J. Zhao, and K. Chen, *J. Electron Spectrosc. Relat. Phenom.* **152**, 143 (2006).
- [35] M. F. Gu, *Can. J. of Phys.* **86**, 675 (2008).
- [36] J. Lewin and P. Smith, *Astropart.Phys.* **6**, 87 (1996).
- [37] S. M. Sze, *Physics of Semiconductor Devices* (John Wiley and Sons, N. Y., 1981).
- [38] H. R. Philipp and E. A. Taft, *Phys. Rev.* **113**, 1002 (1959).
- [39] G. Grilli di Cortona, A. Messina, and S. Piacentini, (2020), [arXiv:2006.02453](https://arxiv.org/abs/2006.02453) [hep-ph].
- [40] J.-W. Chen, H.-C. Chi, K.-N. Huang, C.-P. Liu, H.-T. Shiao, *et al.*, *Phys. Lett. B* **731**, 159 (2014), [arXiv:1311.5294](https://arxiv.org/abs/1311.5294) [hep-ph].
- [41] J.-W. Chen, H.-C. Chi, K.-N. Huang, H.-B. Li, C.-P. Liu, L. Singh, H. T. Wong, C.-L. Wu, and C.-P. Wu, *Phys. Rev. D* **91**, 013005 (2015), [arXiv:1411.0574](https://arxiv.org/abs/1411.0574) [hep-ph].